Biosensors and Bioelectronics 41 (2013) 889–893

Contents lists available at SciVerse ScienceDirect

Biosensors and Bioelectronics

journal homepage: www.elsevier.com/locate/bios

Short communication

Fluorescent aptamer-functionalized graphene oxide biosensor for label-free detection of mercury(II)

Ming Li [a,c], Xuejiao Zhou [b], Weiqiang Ding [c], Shouwu Guo [b], Nianqiang Wu [a,c,*]

[a] Department of Mechanical and Aerospace Engineering, West Virginia University, Morgantown, WV 26506-6106, USA
[b] National Key Laboratory of Micro/Nano Fabrication Technology, Key Laboratory for Thin Film and Microfabrication of the Ministry of Education, Research Institute of Micro/Nano Science and Technology, Shanghai Jiao Tong University, Shanghai 200240, PR China
[c] WV Nano Initiative, West Virginia University, Morgantown, WV 26506, USA

ARTICLE INFO

Article history:
Received 23 July 2012
Received in revised form
16 September 2012
Accepted 25 September 2012
Available online 9 October 2012

Keywords:
Graphene oxide
Mercury
Sensor
Fluorescence
Detection

ABSTRACT

Label-free fluorescent detection of Hg^{2+} has been realized via quenching of fluorescence of graphene oxide (GO). The water-soluble GO sheets, which are functionalized with single-stranded DNA aptamer, exhibit strong fluorescence emission at 600 nm under the excitation of 488 nm in the absence of Hg^{2+} ions. When Hg^{2+} ions appear in the aqueous solution, Hg^{2+} ions are sandwiched between the hairpin-shaped double-stranded DNA due to the formation of the thymine–Hg^{2+}–thymine complex, which holds the Hg^{2+} ions in proximity to the surface of GO sheets. As a result, the fluorescence emission of GO is quenched. The present GO-based sensor shows a limit of detection as low as 0.92 nM and excellent selectivity toward Hg^{2+} over a wide range of metal ions. The present work indicates that GO is a promising fluorescent probe for detection of metal ions and biomolecules.

1. Introduction

Heavy metals are highly toxic and dangerous pollutants. While some heavy metal pollutants come from fertilizers and sewage, industrial waste is the main source of heavy metal pollution (Liu et al., 2011; Nolan and Lippard, 2008; Yilmaz et al., 2007). Mercury is one of the most toxic heavy metals. Even in small concentrations, it is a threat to the environment and human health because it is non-biodegradable. Mercury can enter food chain, posing a threat to human health (Nolan and Lippard, 2008; Vo et al., 2011). Recognition of the toxic effects from minute concentrations of mercury has made it essential to monitor the level of mercury in aquatic environment. The typical inorganic Hg^{2+} level in surface water and groundwater is below 0.5 ppb (WHO, 2011). The maximum allowable Hg^{2+} levels regulated by the U.S. Environmental Protection Agency (EPA) and the international World Health Organization (WHO) are 2 ppb and 6 ppb in drinking water, respectively (WHO, 2011; EPA, 2011). Currently, conventional techniques for Hg^{2+} measurement include inductively coupled plasma mass spectrometry (ICP-MS) (Bings et al., 2006), cold-vapor atomic fluorescence/absorption spectrometry (CV-AFS/CV-AAS) and ultraviolet–visible spectrometry (Lorber, 1986; Kunkel and Manahan, 1973), etc. However, these methods require sophisticated and expensive instruments operated by professionals in a centralized laboratory. In order to overcome these drawbacks, many attempts have been made to develop portable sensors for facile and rapid detection of Hg^{2+}, including colorimetric, electrochemical and fluorescent sensors (Xue et al., 2008; Zhu et al., 2009; Lee et al., 2009, 2007; Lin et al., 2011; Li et al., 2011a, 2011b).

In particular, fluorescent and colorimetric approaches have been used for detection of trace Hg^{2+} with high sensitivity, fast response and easy operation (Lee et al., 2009; Darbha et al., 2007; Guo and Dong, 2011a; Long et al., 2009; Ono and Togashi, 2004). Typically, organic dye molecules have been used as the fluorophores in fluorescent sensors (Ono and Togashi, 2004). However, organic dye molecules are vulnerable to photo-bleaching and exhibit a low quantum yield, and have a narrow light-absorption band range. Therefore, inorganic quantum dots have been employed as alternative fluorophores due to their good resistance against photobleaching, high quantum yields and wide light-absorption band (Li et al., 2011b, Zhao et al., 2011; Wang et al., 2010a; Tan et al., 2003). Unfortunately, inorganic quantum dots typically contain cadmium, selenium, lead or other toxic elements.

Recently, graphene oxide (GO), which contains an environment-friendly, earth-abundant and inexpensive element of carbon, has emerged as a new fluorophore because of its strong photoluminescence, high mechanical strength, good water solubility and facile surface modification capability for bioconjugation (Loh et al., 2010; Wang et al., 2010b). In addition, it has been

* Corresponding author at: Department of Mechanical and Aerospace Engineering, West Virginia University, Morgantown, WV 26506-6106, USA.
Tel.: +1 304 293 3326.
E-mail address: nick.wu@mail.wvu.edu (N. Wu).

0956-5663/$ - see front matter © 2012 Elsevier B.V. All rights reserved.
http://dx.doi.org/10.1016/j.bios.2012.09.060

found that GO can bind single-stranded DNA (ssDNA) via hydrophobic and π–π stacking interactions between the nucleobases and GO (Guo and Irudayaraj, 2011). Therefore, GO can be considered as a promising sensing material (Dong et al., 2010; Jung et al., 2010; Tang et al., 2011; Zhou et al., 2009; Guo and Wang, 2011b; Wu et al., 2004).

Herein, a simple, highly sensitive and selective GO-based fluorescent sensor has been developed for Hg^{2+} detection without the need of complicated, high-cost and time-consuming labeling. In this sensor, GO acts as a fluorophore, and ssDNA aptamer serves as the molecular recognition probe that can selectively bind to Hg^{2+} ions (Ono and Togashi, 2004). To the best of our knowledge, this is the first demonstration of label-free Hg^{2+} detection *via* quenching of the fluorescence emission of GO.

2. Materials and methods

2.1. Chemicals and materials

An aptamer with a sequence of 5′-NH_2-$(CH_2)_6$-TTCTTTCTT-CGCGTTGTTTGTT-3′ can selectively bind to Hg^{2+} ions based on the reported results (Ono and Togashi, 2004). The Hg^{2+} specific-DNA aptamer was purchased from Integrated DNA Technologies (IDT, Coralville, IA). N-hydroxysuccinimide (NHS), 1-ethyl-3-(3-dimethylaminopropyl)-carbodiimide (EDC), $Cu(NO_3)_2$, $Hg(NO_3)_2$, $Pb(NO_3)_2$, $Cd(NO_3)_2 \cdot 4H_2O$, $Co(NO_3)_2 \cdot 6H_2O$ and 5 M NaCl stock solution were purchased from Sigma-Aldrich (St. Louis, MO). KI (99.9%), $AgNO_3$ (Premion, 99.995%), $Fe(NO_3)_3 \cdot 9H_2O$, $Ni(NO_3)_2 \cdot 6H_2O$, Na_2HPO_4 (99.0%), NaH_2PO_4 (99.0%) and ethylenediamine (99%) were obtained from Alfa-Aesar (Ward Hill, MA). Deionized (D.I.) water produced by a Milli-Q Millipore system (18.2 MΩ cm, Millipore Corp., Billerica, MA) was used for the preparation of all the solutions. All chemicals and solvents were obtained from the commercial sources and used directly without any further purification.

2.2. Preparation of ssDNA–GO conjugates

GO was prepared according to the well-established Hummers method (Hummers and Offeman, 1958; Ren et al., 2010; Zhang et al., 2010; Zhou et al., 2011). The as-prepared GO was dispersed in a 10 mM PBS solution (0.3 M NaCl, pH = 7.0) through ultrasonication for 4 h to obtain a suspension containing 2.0 mg/mL GO. For functionalization of GO by ssDNA, 1 mL of 50 mM NHS and 200 mM EDC in 10 mM PBS was added to 1 mL of 2.0 mg/mL GO suspension, and the mixture was kept standing for 2 h. Afterwards, 20 nM ssDNA was added, and the mixture was incubated overnight. The excessive and free ssDNA aptamer was removed by centrifugation and washing with 10 mM PBS, and the mixture was then re-dispersed into 10 mM PBS solution to obtain a concentration of 100 μg/mL for further use. As a result, the aptamer was immobilized on the GO sheet with a certain amount (around 10 nmol aptamer per gram of GO) based on the measurement of absorption spectroscopy of the aptamer solution (Fig. S1).

2.3. Instrumentation and characterization

UV–visible absorption spectra were recorded with a Shimadzu UV-2550 spectrometer (Shimadzu Co., Kyoto, Japan). The fluorescence (FL) spectra were collected with a HITACHI F-7000 fluorescence spectrophotometer (Hitachi High-Tech, Tokyo, Japan) under excitation of 488 nm (950 V PMT voltage, 10 nm excitation and emission slits, and 0.02 s response time). The GO sheet were observed under the tapping mode atomic force microscopy (AFM) using a nanoscope multiMode scanning probe microscope (Bruker/Digital Instrument, Santa Barbara, CA). The samples for AFM measurement were prepared by depositing a drop of aqueous GO solution on a freshly cleaved mica surface and drying at room temperature. Fourier transform infrared (FT-IR) spectra were obtained under a transmission mode with a Nicolet 6700 spectrometer (Thermo Scientific, Waltham, MA). Raman spectra measurement was carried out with a Renishaw invia Raman spectrometer (Renishaw PLC, Gloucestershire, UK) under excitation of the 532 nm laser with a 20× objective lens. X-ray photoelectron spectra (XPS) were acquired with a PHI 5000 Versa Probe system (Physical Electronics, MN).

2.4. Hg^{2+} detection experiments

The assay solution contained 100 μg/mL aptamer–GO conjugates (or GO), 0.3 M NaCl and 0.1 mM ethylenediamine in 10 mM phosphate-buffered saline (PBS) solution (pH = 7.0). The time-dependent fluorescence spectra were monitored after 20 nM Hg^{2+} was added into the assay solution. For the sensitivity measurement, different concentrations (0, 0.1, 0.2, 0.5, 1, 2, 10, 20, 50, 100, 500 and 1000 nM) of Hg^{2+} were added to the assay solution, and the fluorescence spectra were recorded. The selectivity was checked by addition of 200 nM K^+, Ag^+, Ca^{2+}, Cd^{2+}, Cu^{2+}, Pb^{2+}, Ni^{2+}, Co^{2+} and Fe^{3+}. The effect of the ionic strength on the aptamer–Hg^{2+} binding was investigated at various NaCl concentrations (0.01, 0.1, 0.3 and 0.75 M).

3. Results and discussion

Fig. 1(a) shows an AFM image of the bare GO sheets dispersed on the mica. The line-profile across a single GO sheet reveals that it was around 1.2 nm thick, indicating a monolayer GO sheet (Loh et al., 2010). Fig. 1(b) shows the FT-IR spectrum of the bare GO sheets. The absorption bands at 3411 cm^{-1} and 1734 cm^{-1} were characteristic of the O–H stretching vibration and the C=O stretching vibration, respectively (Wu et al., 2004; Lim et al., 2007). The bands at 1621, 1198 and 1053 cm^{-1} were assigned to the benzene ring skeletal vibration of graphitic carbon, C–OH stretching vibration and C–O stretching mode, respectively (Xiang et al., 2012; Wu et al., 2004; Ren et al., 2010). The FT-IR peaks at 854 cm^{-1} and 586 cm^{-1} were assigned to the epoxide bending and the C–H bond in the benzene ring, respectively (Mathkar et al., 2012; Kumar et al., 2012). The above results demonstrated that the GO used in the present study was a monolayer sheet with oxygen-containing functional groups. The Raman spectrum in Fig. 1(c) displayed the D and G bands at 1350 and 1598 cm^{-1}, respectively (Xiang et al., 2012). It is well-known that GO has excellent water solubility due to the oxygen-containing functional groups, which also enables the facile functionalization of biomolecules such as proteins and DNA. In the present work, the aptamer–GO conjugates were made by the well-established carbodiimide chemistry. The XPS spectra confirmed that aptamer was attached to the GO sheets (Fig. S2).

Fig. 1(d, e) shows the fluorescence emission at 600 nm for the aptamer-functionalized GO in the PBS solution. In contrast to graphene, GO contains various oxygen-containing functional groups that create a band gap in the GO sheets. The band gap of GO depends on the nature and the fraction of sp^2 carbon atoms. Tuning the sp^2/sp^3 carbon atomic ratio can effectively tune the band gap of GO, varying the photoluminescence. The operation principle of label-free Hg^{2+} detection is illustrated in Scheme 1. In the absence of Hg^{2+}, the ssDNA aptamer molecules lay down on the surface of the GO sheets in a flexible manner (Zhang et al., 2011; Wu et al., 2011). When Hg^{2+} ions are present, a rigid hairpin-shaped double-stranded DNA structure is formed due to the coordination of T-Hg^{2+}-T

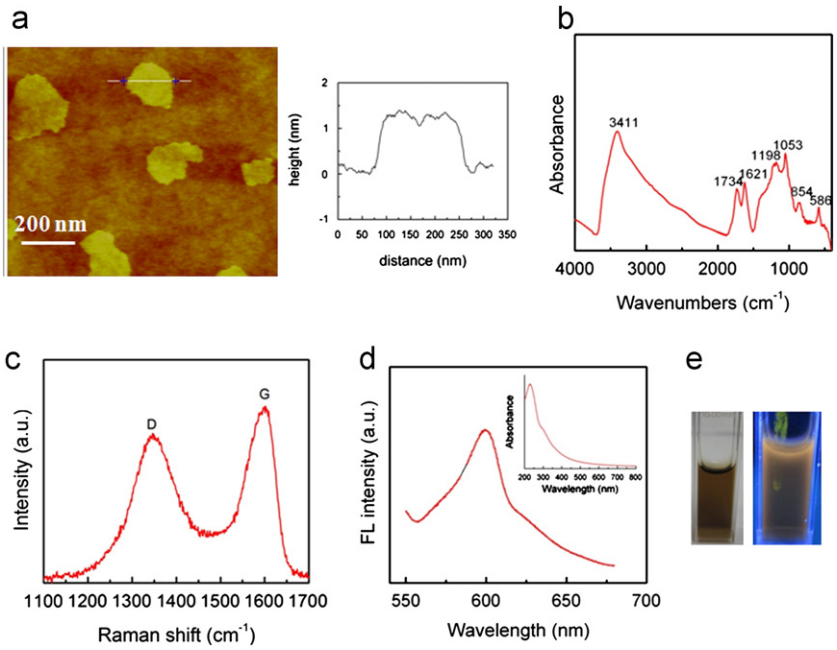

Fig. 1. (a) Tapping mode AFM image of the bare GO sheets and the height profile; (b) FT-IR spectrum and (c) Raman spectrum of the bare GO sheets; (d) fluorescence spectrum of the aptamer-functionalized GO sheets in the PBS solution (Inset: UV–visible absorption spectrum); and (e) optical pictures of the aptamer-functionalized GO sheets in PBS solution under the excitation of sunlight (left) and 365 nm light (right).

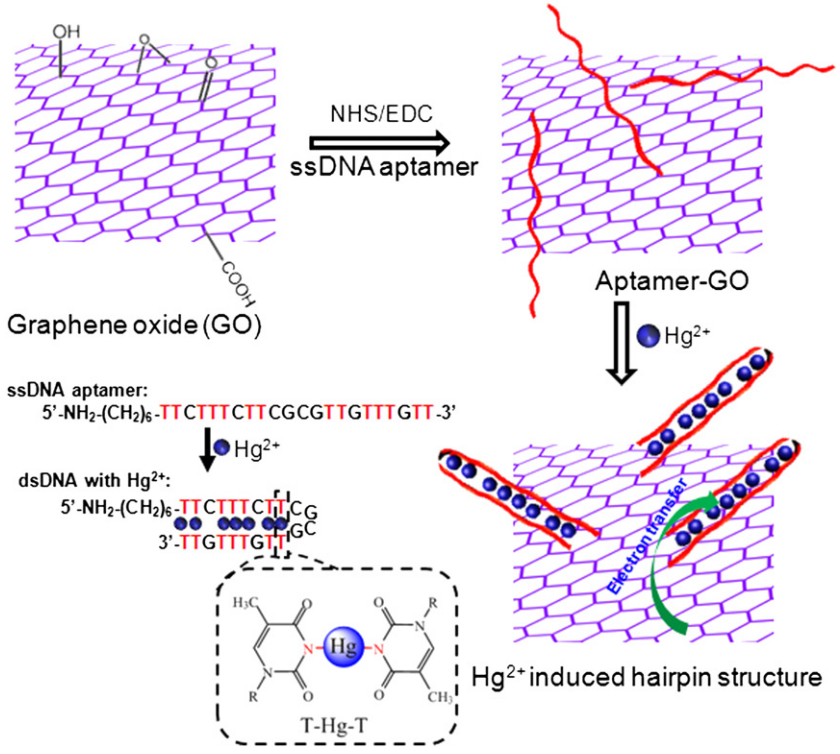

Scheme 1. Operation principle of the label-free detection of Hg^{2+} based on quenching of the fluorescence emission of graphene oxide.

(Ono and Togashi, 2004). The Hg^{2+} ions are very close to the surface of the GO sheet (the closest Hg^{2+} ion are less than 1 nm away). Therefore, electrons can transfer from GO to the Hg^{2+} ions along the duplex DNA channel (Freeman et al., 2009; Haas et al., 2004), which results in the quenching of fluorescence emission of GO. The detection mechanism is based on the "turn-off" of the fluorescence of GO.

The fluorescence quenching kinetics of the aptamer–GO conjugates in a PBS solution (10 mM Na_2HPO_4/NaH_2PO_4, 0.3 M NaCl, 0.1 mM ethylenediamine, pH = 7.0) was examined in the presence of 20 nM Hg^{2+} (Fig. S3). It was found that the fluorescence intensity decreased quickly with prolonging of the incubation time, and reached a steady-state after about 5 min. In other words, the conformation change of the aptamer was completed

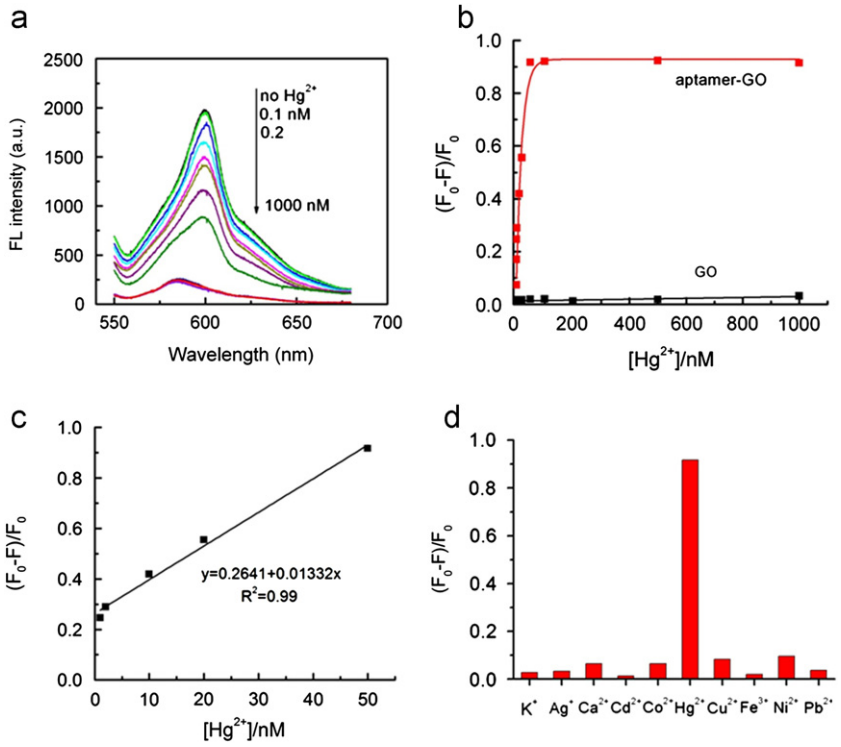

Fig. 2. (a) Fluorescence spectra of the aptamer–GO conjugates in the assay solution containing various concentrations (0, 0.1, 0.2, 0.5, 1, 2, 10, 20, 50, 100, 500 and 1000 nM) of Hg^{2+} ions; (b) plot of the fluorescence intensity at 600 nm as a function of the Hg^{2+} concentration; (c) the linear region of sensing response; and (d) quenching efficiency of fluorescence in the presence of various metal ions. $[Hg^{2+}]=50$ nM and other metal ions have a concentration of 200 nM.

after the steady-state was reached. It was worth noting that the ionic strength had significant effect on the binding of the aptamer to Hg^{2+} (Fig. S4). At a low NaCl level (0.01 and 0.1 M) in the PBS solution, the aptamer was not able to bind to Hg^{2+}, leading to negligible change in the fluorescence in the presence of Hg^{2+}. In the present work, 0.3 M NaCl was selected for the optimal ionic strength. In addition, we evaluated the fluorescence response of the unfunctionalized GO to the presence of various concentrations of Hg^{2+}. There was no observable change in the fluorescence intensity even after 1 μM Hg^{2+} ions were added into the assay containing the bare GO sheets (Fig. S5). In contrast, the fluorescence intensity of the assay containing the aptamer-functionalized GO was very sensitive to the presence of Hg^{2+} ions (Fig. 2(a)). Fig. 2(b) shows the calibration plot of the quenching efficiency (F/F_0) as a function of the Hg^{2+} concentration, where F_0 and F are the fluorescence intensities at 600 nm before and after various concentrations of Hg^{2+} are added, respectively. The fluorescence intensity decreased with an increase in the concentration of Hg^{2+} ions, and reached the saturation up to 50 nM (Fig. 2(b)). A linear dynamic range was observed from 1 nM to 50 nM (Fig. 2(c)). The limit of detection (LOD) was determined to be 0.92 nM (0.18 ppb), which was one order lower than the maximum allowable levels of Hg^{2+} in drinking water regulated by the international World Health Organization (6 ppb) and the U.S. Environmental Protection Agency (2 ppb). The LOD of the present sensor was better or comparable to the best fluorescent, electrochemical and colorimetric sensors reported previously.

Furthermore, the selectivity of the present sensor toward Hg^{2+} was tested. Fig. 2(d) shows the fluorescence response of the sensor to the presence of various metal ions, including K^+, Ag^+, Ca^{2+}, Cd^{2+}, Cu^{2+}, Pb^{2+}, Ni^{2+}, Co^{2+} and Fe^{3+}. No obvious fluorescence intensity change was observed in the presence of other metal ions. Therefore, the sensor exhibited excellent selectivity, which was mainly attributed to the high specificity of the thymine base toward Hg^{2+}.

4. Conclusions

In summary, the ssDNA aptamer attached on GO can specifically bind to the Hg^{2+} ion through the formation of T–Hg^{2+}–T complexes, leading to the formation of a hairpin-shaped double-stranded DNA structure. The Hg^{2+} ions intercalated in the double-stranded DNA are in close proximity to the surface of GO sheets, leading to the quenching of the fluorescence of GO. This sensing approach has several unique features. Firstly, it is a label-free detection approach, which saves the cost and simplifies the operation of the sensor. Secondly, the assay time is very short (only 5 min). Thirdly, the sensor exhibits a limit of detection as low as 0.92 nM and excellent selectivity toward Hg^{2+} when co-existing with other metal ions. It is believed that this sensing strategy can be extended to detection of other metal ions and biomolecules.

Acknowledgment

This work was financially supported by a NSF Grant (CBET-0754405). The resource and facilities used were partially supported by NSF (EPS 1003907) and a Research Challenge Grant from the State of West Virginia (EPS08-01), the West Virginia University Research Corporation and the West Virginia EPSCoR Office. We are grateful to the use of the WVU Shared Research Facilities.

Appendix A. Supporting information

Supplementary data associated with this article can be found in the online version at http://dx.doi.org/10.1016/j.bios.2012.09.060.

References

Bings, N.H., Bogaerts, A., Broekaert, J.A.C., 2006. Analytical Chemistry 78, 3917–3946.
Darbha, G.K., Ray, A., Ray, P.C., 2007. ACS Nano 1, 208–214.
Dong, H., Gao, W., Yan, F., Ji, H., Ju, H., 2010. Analytical Chemistry 82, 5511–5517.
EPA, U.S., Drinking Water Contaminants, 〈http://water.epa.gov/drink/contaminants/index.cfm#List〉. (Accessed on 31 12 11).
Freeman, R., Finder, T., Willner, I., 2009. Angewandte Chemie-International Edition 48, 7818–7821.
Guo, C., Irudayaraj, J., 2011. Analytical Chemistry 83, 2883–2889.
Guo, S., Dong, S., 2011a. Journal of Materials Chemistry 21, 18503–18516.
Guo, S., Wang, E., 2011b. Accounts of Chemical Research 44, 491–500.
Haas, C., Kräling, K., Cichon, M., Rahe, N., Carell, T., 2004. Angewandte Chemie 116, 1878–1880.
Hummers, W.S., Offeman, R.E., 1958. Journal of the American Chemical Society 80, 1339.
Jung, J.H., Cheon, D.S., Liu, F., Lee, K.B., Seo, T.S., 2010. Angewandte Chemie-International Edition 49, 5708–5711.
Kumar, N.A., Choi, H.J., Shin, Y.R., Chang, D.W., Dai, L., Baek, J.B., 2012. ACS Nano 6, 1715–1723.
Kunkel, R., Manahan, S.E., 1973. Analytical Chemistry 45, 1465–1468.
Lee, J., Jun, H., Kim, J., 2009. Advanced Materials 21, 3674–3677.
Lee, J., Han, M.S., Mirkin, C.A., 2007. Angewandte Chemie-International Edition 46, 4093–4096.
Li, M., Cushing, S.K., Wang, Q., Shi, X., Hornak, L.A., Hong, Z., Wu, N., 2011a. Journal of Physical Chemistry Letters 2, 2125–2129.
Li, M., Wang, Q., Shi, X., Hornak, L.A., Wu, N., 2011b. Analytical Chemistry 83, 7061–7065.
Lim, M.S., Feng, K., Chen, X.Q., Wu, N.Q., Raman, A., Gawalt, E.S., Nightingale, J., Korakakis, D., Hornak, L.A., Timperman, A., 2007. Langmuir 23, 2444–2452.
Lin, Z., Li, X., Kraatz, H.B., 2011. Analytical Chemistry 83, 6896–6901.
Liu, Q., Peng, J., Sun, L., Li, F., 2011. ACS Nano 5, 8040–8048.
Loh, K.P., Bao, Q., Eda, G., Chhowalla, M., 2010. Nature Chemistry 2, 1015–1024.
Long, Y., Jiang, D., Zhu, X., Wang, J., Zhou, F., 2009. Analytical Chemistry 81, 2652–2657.
Lorber, K.E., 1986. Waste Management & Research 4, 3–13.
Mathkar, A., Tozier, D., Cox, P., Ong, P., Galande, C., Balakrishnan, K., Reddy, A.L.M., Ajayan, P.M., 2012. Journal of Physical Chemistry Letters 3, 986–991.
Nolan, E.M., Lippard, S.J., 2008. Chemical Reviews 108, 3443–3480.
Ono, A., Togashi, H., 2004. Angewandte Chemie-International Edition 43, 4300–4302.
Ren, H., Wang, C., Zhang, J., Zhou, X., Xu, D., Zheng, J., Guo, S., Zhang, J., 2010. ACS Nano 4, 7169–7174.
Tan, G.L., Hommerich, U., Temple, D., Wu, N.Q., Zheng, J.G., Loutts, G., 2003. Scripta Materialia 48, 1469–1474.
Tang, D., Tang, J., Li, Q., Su, B., Chen, G., 2011. Analytical Chemistry 83, 7255–7259.
Vo, A.T.E., Bank, M.S., Shine, J.P., Edwards, S.V., 2011. Proceedings of the National Academy of Sciences USA 108, 7466–7471.
Wang, D., Zhao, H., Wu, N.Q., Khakani, A.E., Ma, D., 2010a. Journal of Physical Chemistry Letters 1, 1030–1035.
Wang, Y., Li, Z., Hu, D., Lin, C.T., Li, J., Lin, Y., 2010b. Journal of the American Chemical Society 132, 9274–9276.
WHO Guidelines for drinking-water quality, World Health Organization, 4th edn. 2011.
Wu, M., Kempaiah, R., Huang, P.J.J., Maheshwari, V., Liu, J., 2011. Langmuir 27, 2731–2738.
Wu, N.Q., Fu, L., Su, M., Aslam, M., Wong, K.C., Dravid, V.P., 2004. Nano Letters 4, 383–386.
Xiang, C., Li, M., Zhi, M., Manivannan, A., Wu, N.Q., 2012. Journal of Materials Chemistry 22, 19161–19167.
Xue, X., Wang, F., Liu, X., 2008. Journal of the American Chemical Society 130, 3244–3245.
Yilmaz, F., Özdemir, N., Demirak, A., Tuna, A.L., 2007. Food Chemistry 100, 830–835.
Zhao, H., Chaker, M., Wu, N.Q., Ma, D., 2011. Journal of Materials Chemistry 21, 8898–8904.
Zhang, J., Yang, H., Shen, G., Cheng, P., Zhang, J., Guo, S., 2010. Chemical Communications 46, 1112–1114.
Zhang, M., Yin, B.C., Tan, W., Ye, B.C., 2011. Biosensors and Bioelectronics 26, 3260–3265.
Zhou, M., Zhai, Y., Dong, S., 2009. Analytical Chemistry 81, 5603–5613.
Zhou, X., Zhang, J., Wu, H., Yang, H., Zhang, J., Guo, S., 2011. Journal of Physical Chemistry C 115, 11957–11961.
Zhu, Z., Su, Y., Li, J., Li, D., Zhang, J., Song, S., Zhao, Y., Li, G., Fan, C., 2009. Analytical Chemistry 81, 7660–7666.